Experiment N-SI-131, ALTO IJCLab, March 2023

Evidence for enhanced collectivity in ^{58}Fe examined through Coulomb excitation

Giorgia Pasqualato

Joa Ljungvall

Andrew Stuchbery

NuBall2 workshop, 4 July 2024, Milano

Onset of deformation below neutron-rich Ni isotopes

^{58}Fe (Z=26) is placed at the border of a region of the nuclear chart where a development of collectivity has been observed and predicted*.

+

Proximity to the Z=28, N=40 doubly-magic nucleus ^{68}Ni.

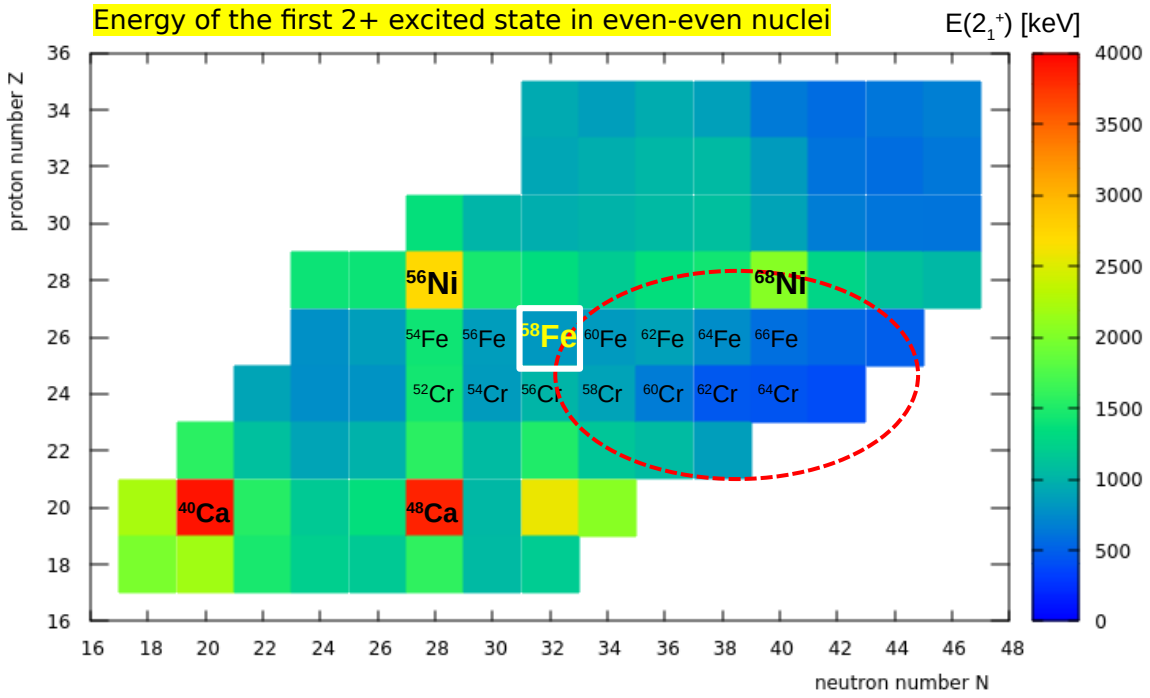

*J. Ljungvall et al., Phys. Rev. C 81 (2010) 061301.
*S. M. Lenzi, F. Nowacki, A. Poves and K. Sieja, Phys. Rev. C 82 (2010) 054301.

Onset of deformation below neutron-rich Ni isotopes

^{58}Fe (Z=26) is placed at the border of a region of the nuclear chart where a development of collectivity has been observed and predicted*.

+

Proximity to the Z=28, N=40 doubly-magic nucleus ^{68}Ni.

Contrast between two opposite behaviors:

- Collectivity: nuclear states can be described as the collective motion (the interaction) between many valence nucleons.
  → **easy to excite**

- Single-particle: only few nucleons are involved on the definition of the nuclear states wave functions
  → **pretty stable over excitation**

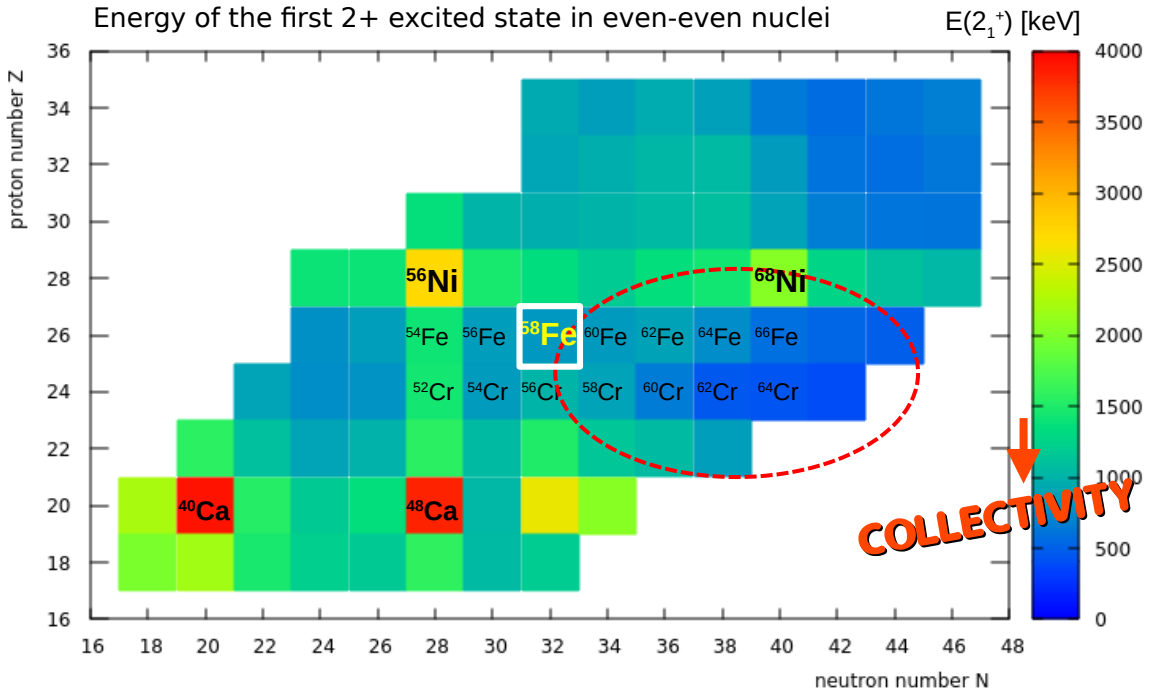

Fingerprints of collectivity in nuclei:

- Small E(2$^+$)
- Large B(E2)

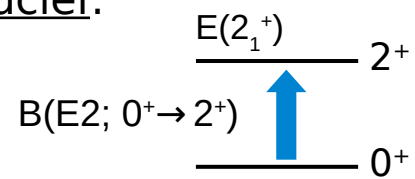

Onset of deformation below neutron-rich Ni isotopes

Microscopic explanation :

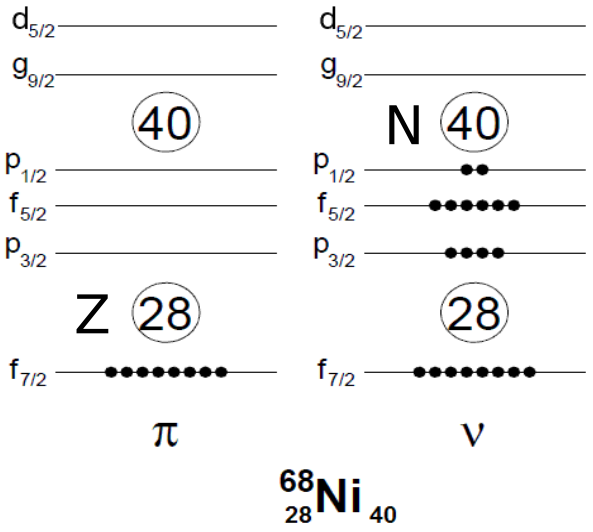

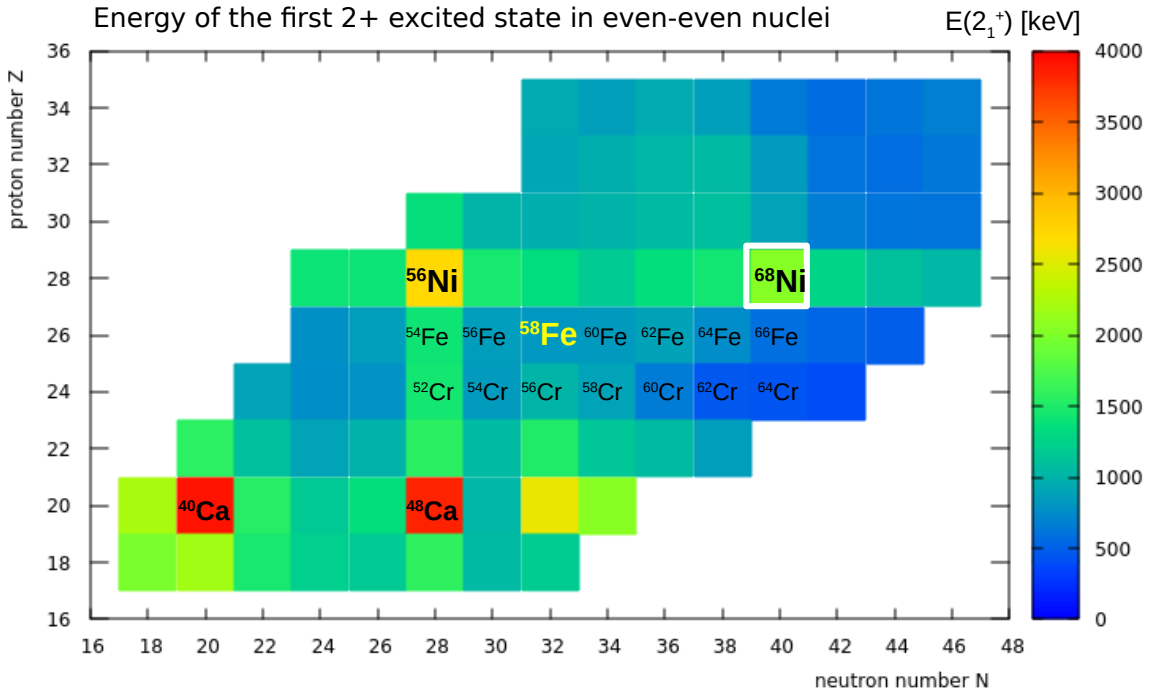

Onset of deformation below neutron-rich Ni isotopes

Microscopic explanation :

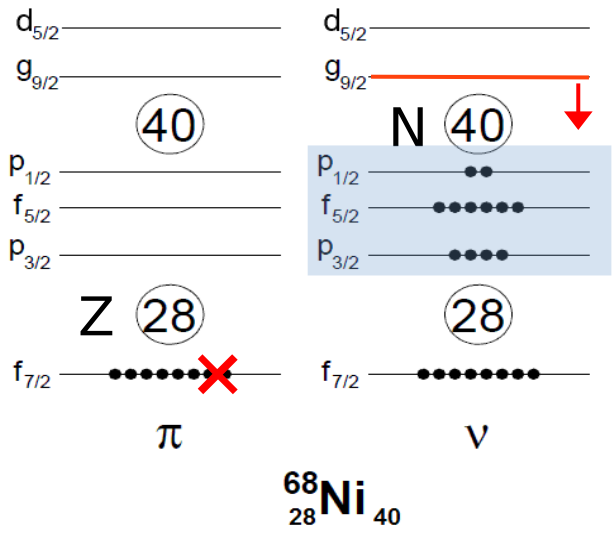

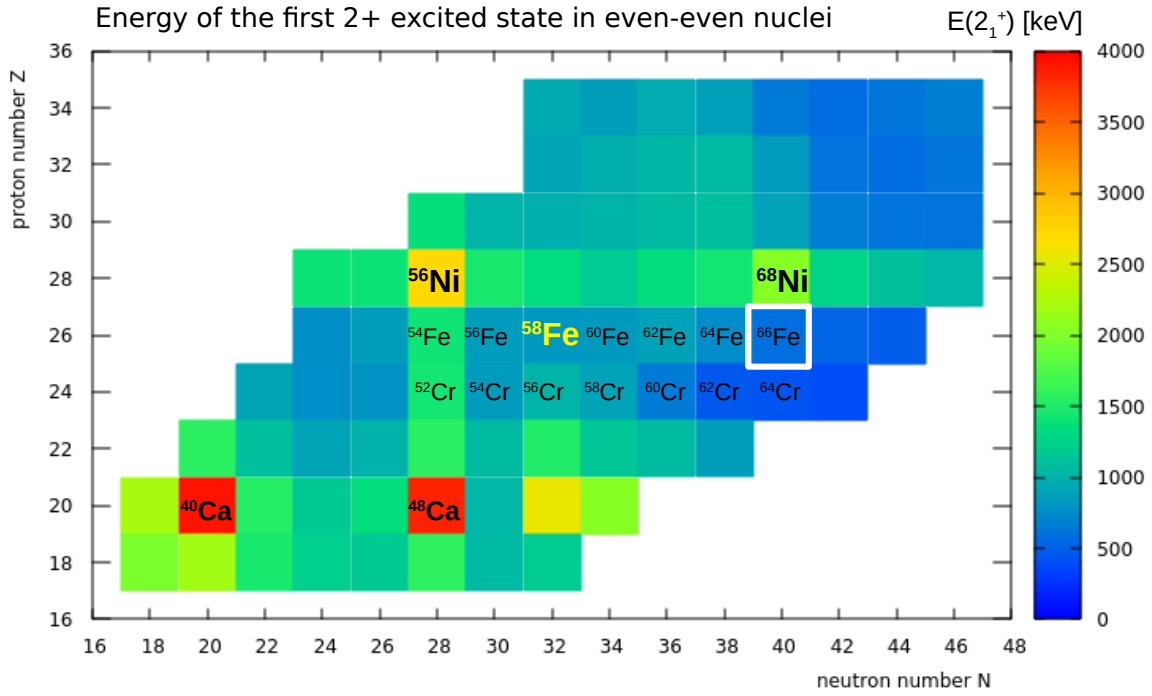

Removing 2 protons from the $f_{7/2}$ orbital implies a re-distribution of neutron orbitals in the *fp* shell with the lowering of the $g_{9/2}$ orbital

→ enhancement of correlations between neutrons and protons

→ **increased collectivity**

Onset of deformation below neutron-rich Ni isotopes

Microscopic explanation :

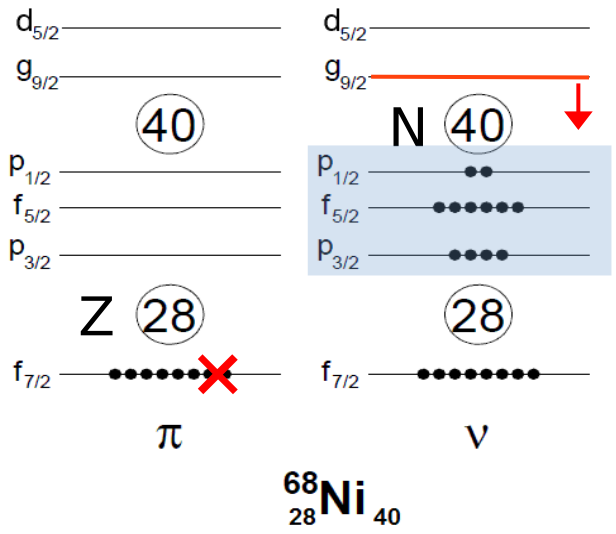

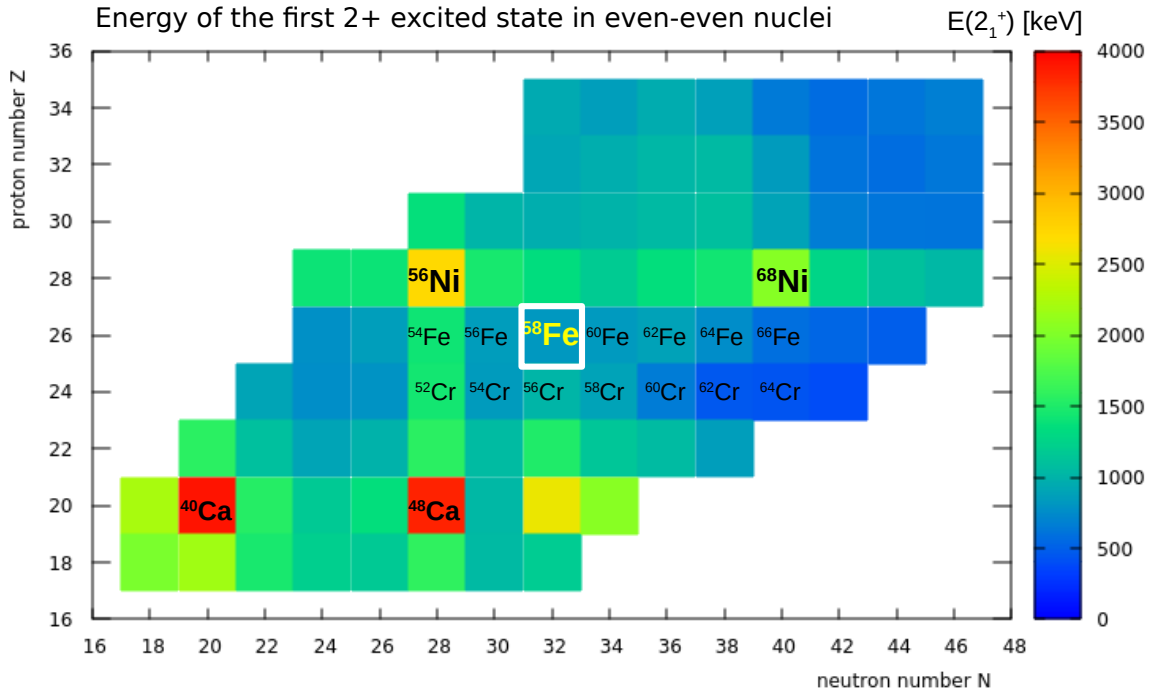

To study this mechanism and understand its microscopic origin, other than the energy of the first excited state, more sensitive probes needs to be investigated, such as reduced transition probabilities.

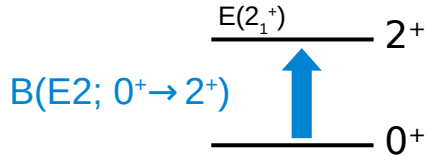

Low-lying energies in Cr and Fe isotopes

This region is accessible by different theoretical models, e.g. by the interacting shell model (ISM) and the interacting boson model (IBM-2)*.

*J. Kotila and S. M. Lenzi, Phys. Rev. C 89 (2014) 064304.

The calculated energy of the first excited states for iron isotopes are supported by experimental data.

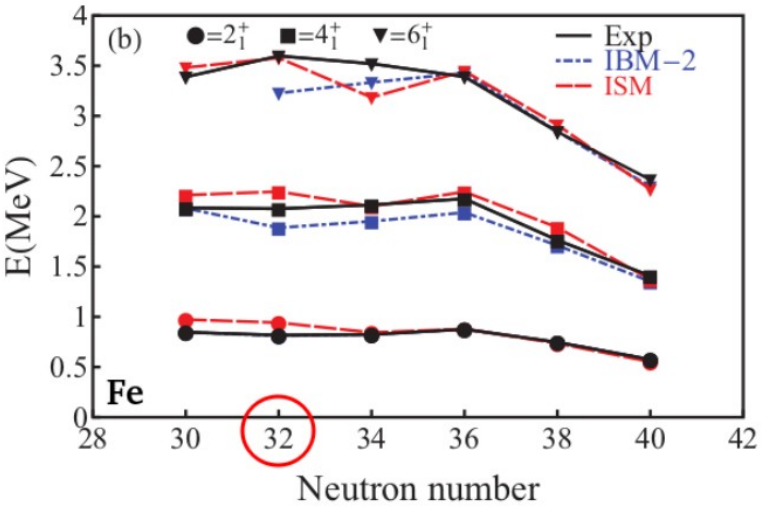

Low-lying energies in Cr and Fe isotopes

This region is accessible by different theoretical models, e.g. by the interacting shell model (ISM) and the interacting boson model (IBM-2)*.

*J. Kotila and S. M. Lenzi, Phys. Rev. C 89 (2014) 064304.

The calculated energy of the first excited states for iron isotopes are supported by experimental data.

The value of transition probabilities show the increase of collectivity going towards N=40.

Experimental data support the model predictions, however...

Large disagreement for the B(E2; $4_1^+ \rightarrow 2_1^+$) at N=32.

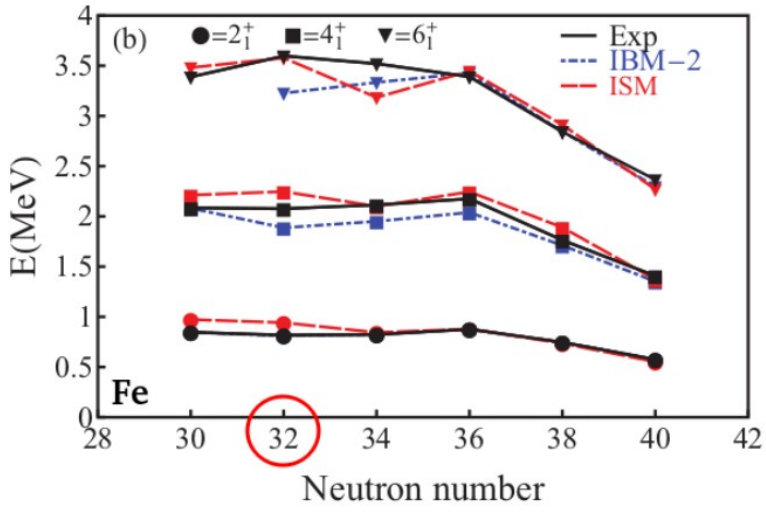

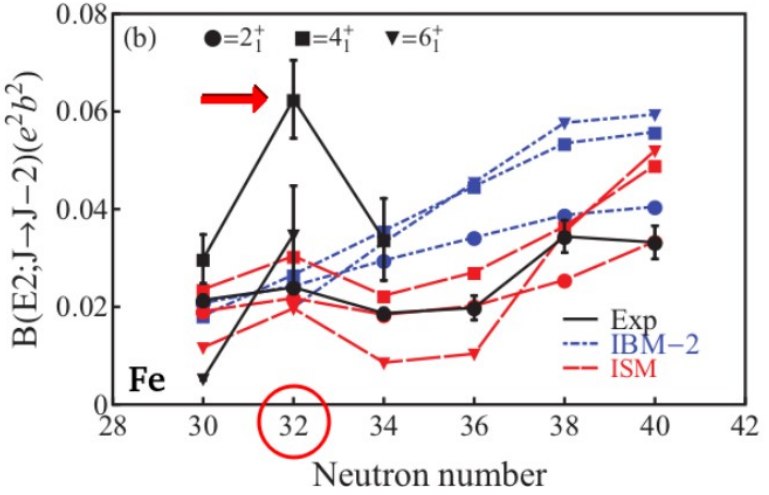

The ^{58}Fe case: B(E2; $4^+ \longrightarrow 2^+$) value

Two possible scenarios:

- The adopted value is wrong.

- Something not included in the calculations is at play for this state.

The ^{58}Fe case: B(E2; $4^+ \longrightarrow 2^+$) value

Two possible scenarios:

- The adopted value is wrong.
  - The B(E2; $4^+ \rightarrow 2^+$) has been obtained only via lifetime measurements.
    τ = 0.53(9) ps using the 55Mn(α, p)58Fe reaction, is the closest to the one predicted

    *Andrew Stuchbery, Honours Thesis, University of Melbourne (1977).

- Something not included in the calculations is at play for this state.

The B(E2; $4^+ \rightarrow 2^+$) can be studied via multi-step Coulomb excitation.

→ ^{58}Fe has been already studied in Coulomb excitation, but limiting excitation to the 2^+ state.

Coulomb-excitation experiments

How does it work?

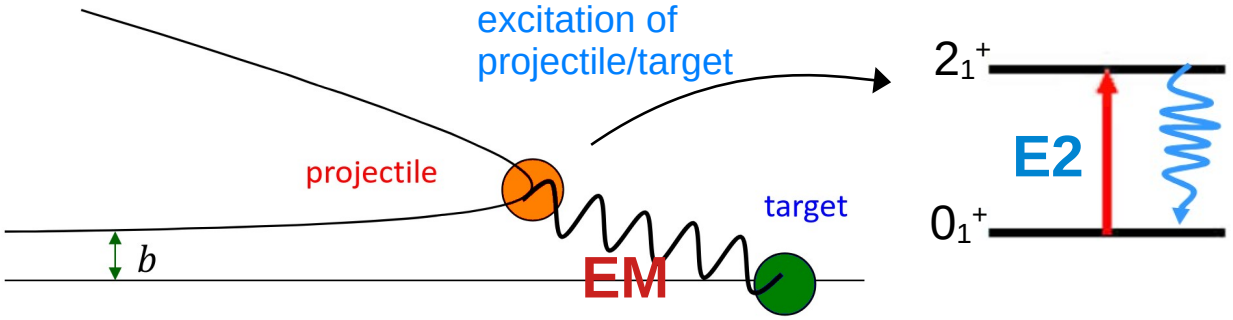

The matrix elements **$\langle J_f||E2||J_i\rangle$** describe the excitation and decay process.

→ they are directly related to **γ-ray intensities** observed in the spectra.

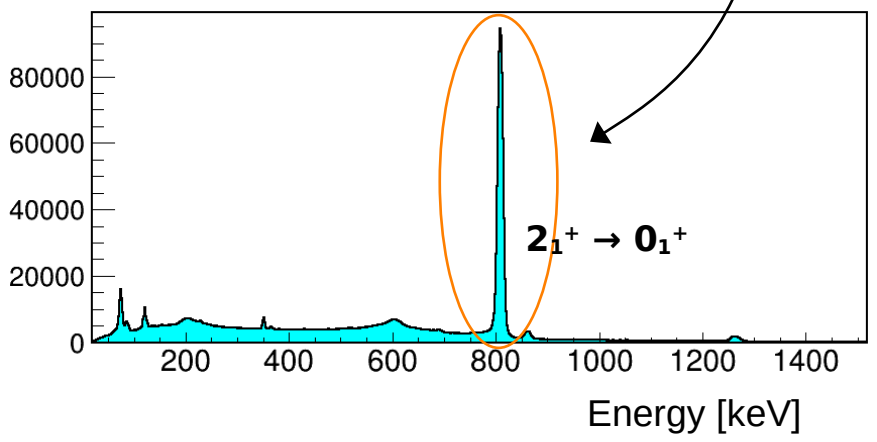

What can we measure?

- the reduced transition probability B(E2; $4_1^+ \rightarrow 2_1^+$).
- Measure the quadrupole moment of the 2_1^+ state.
- Measure the β_2, γ deformation parameters to infer the shape of the g.s.

Coulomb-excitation experiments

SCCM : Simmetry Conserving Configuration Mixing model

Collective wave functions

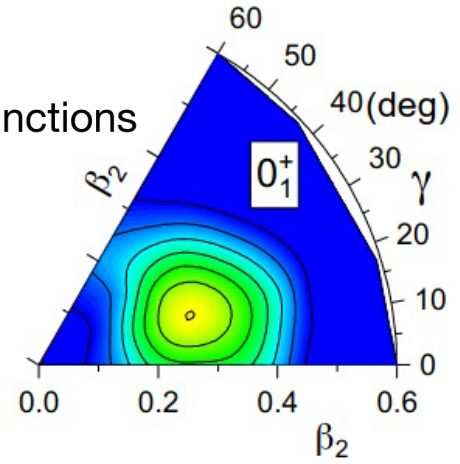

ground state band 0+, 2+, 4+, etc., built on top of a **triaxial-prolate** state

Tomás R. Rodríguez

What can we measure?

- the reduced transition probability B(E2; $4_1^+ \rightarrow 2_1^+$).
- Measure the quadrupole moment of the 2_1^+ state.
- Measure the β_2, γ deformation parameters to infer the shape of the g.s.

Total Energy Surface (TES)

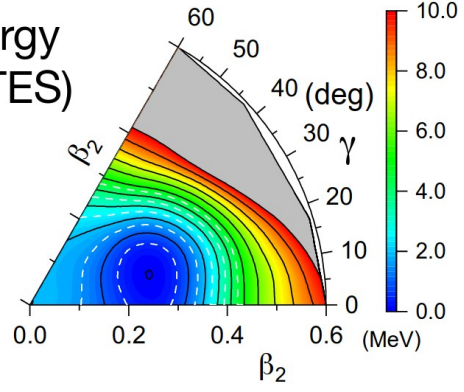

Proposed experiment : multi-step Coulomb excitation

Beam: ^{58}Fe, energy 220 MeV.

Beam prepared with a high enrichment of ^{58}Fe.
→ The beam energy respects the Cline safe-energy criteria

Target: ^{208}Pb, 2 mg/cm^2, self supporting.

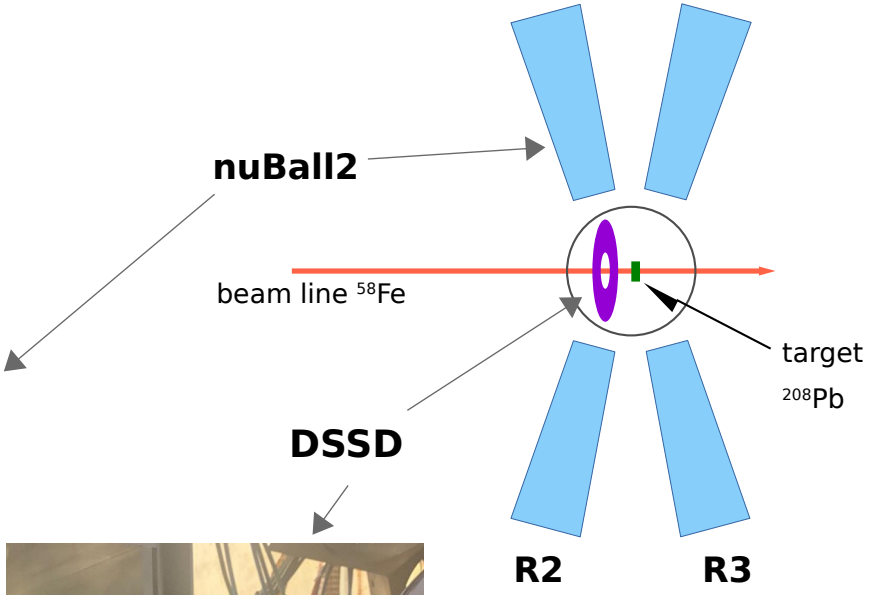

Experimental setup :

● **nuBall2** :

2 rings of 12+12 Compton-suppressed clovers of HPGe.

● **HIL-Warsaw DSSSD** :

highly-segmented Si detector at backward angles.

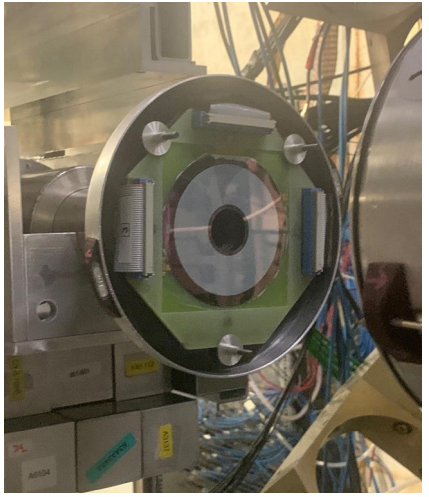

The HIL-Warsaw **DSSSD** (Double-Sided Stripped Silicon Detector)

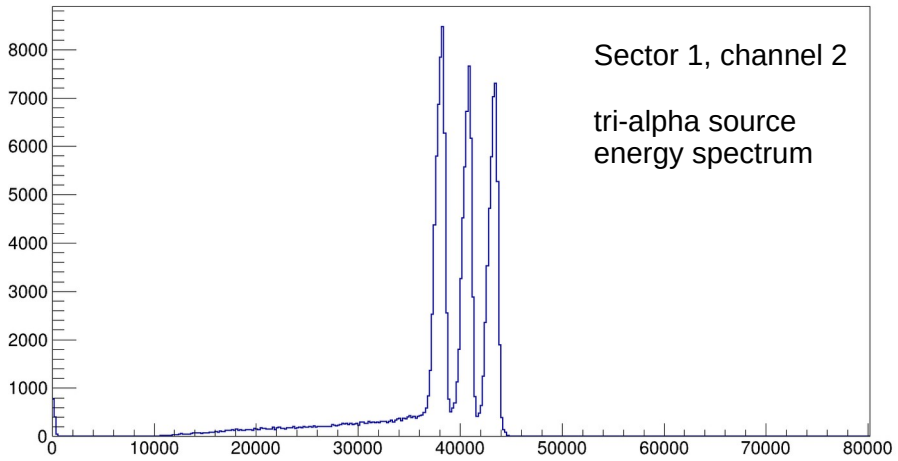

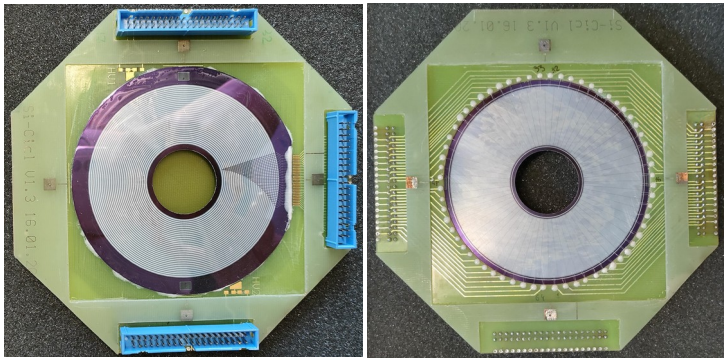

DSSD spectra each channel 1 ring et 1 sector in coincidence

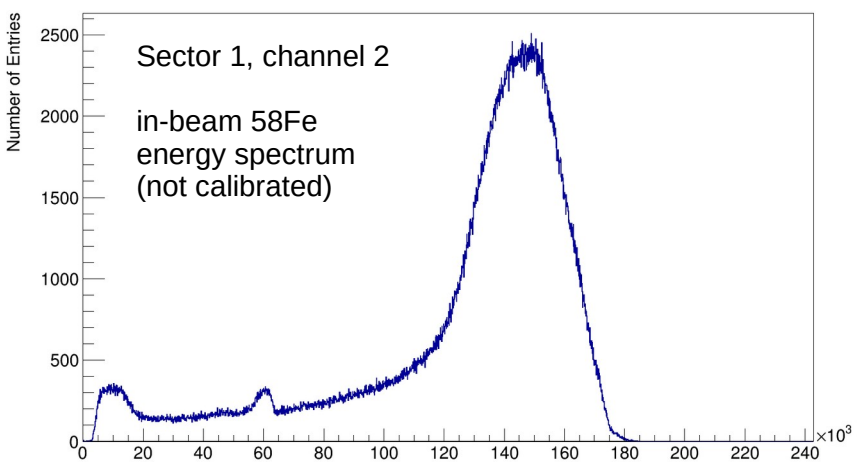

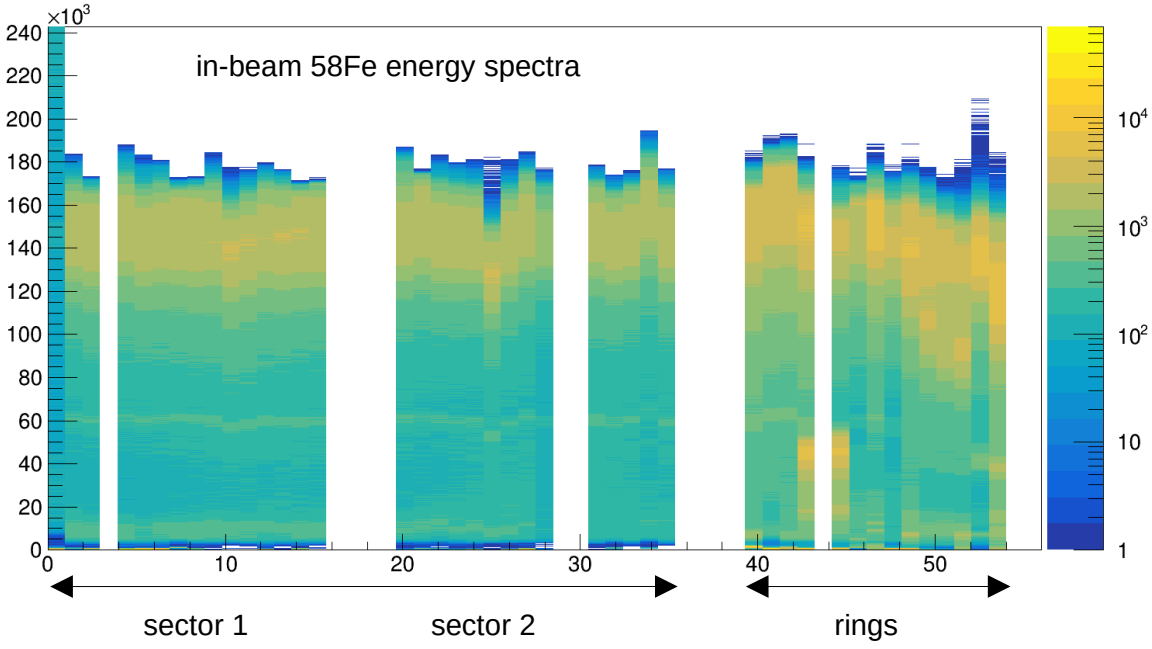

Data presorting – Energy calibration of HPGe

Linear correction for all runs using the 152Eu source + correction of the gain shift using the most intense peaks in the spectra for each run.

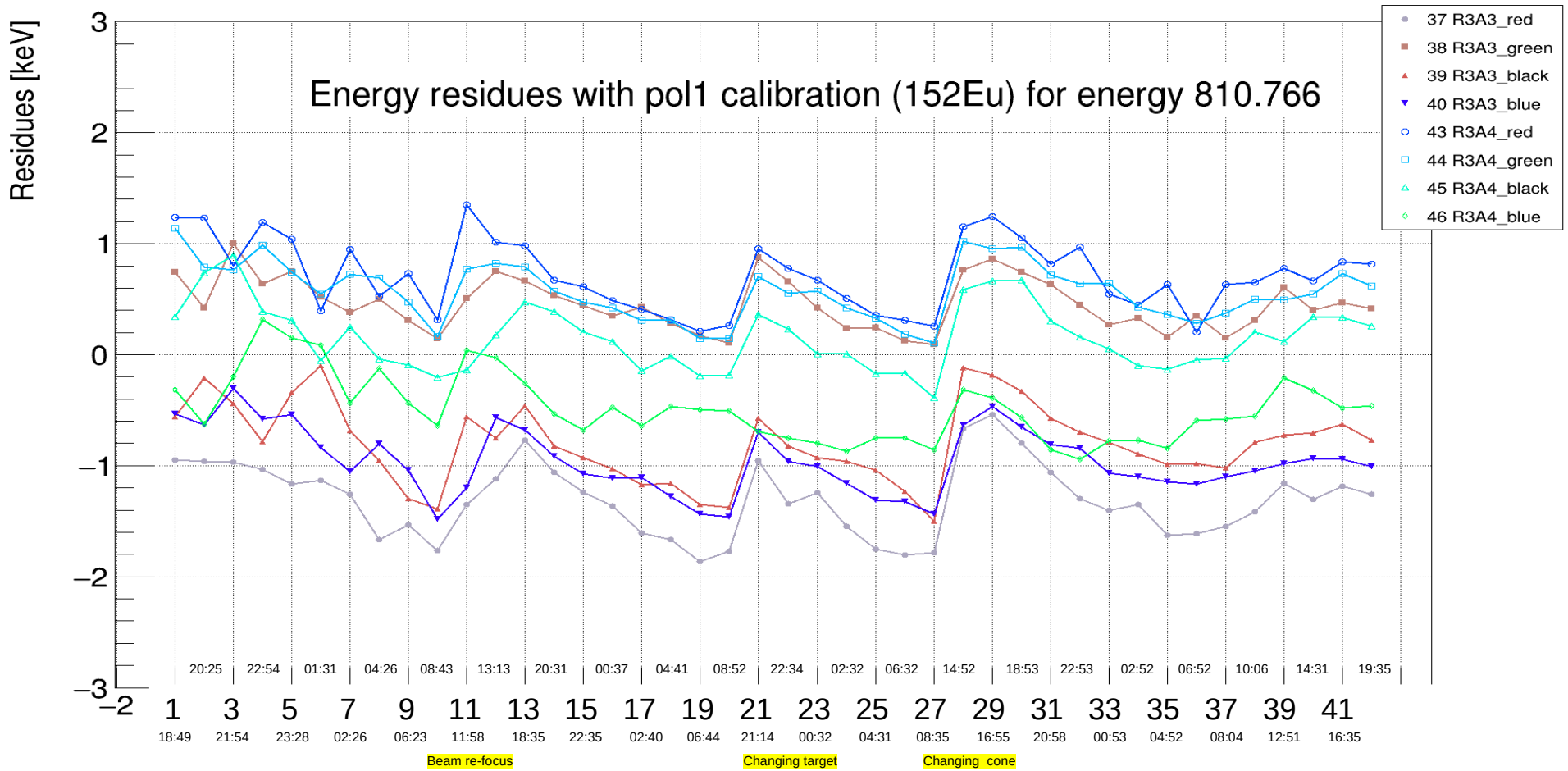

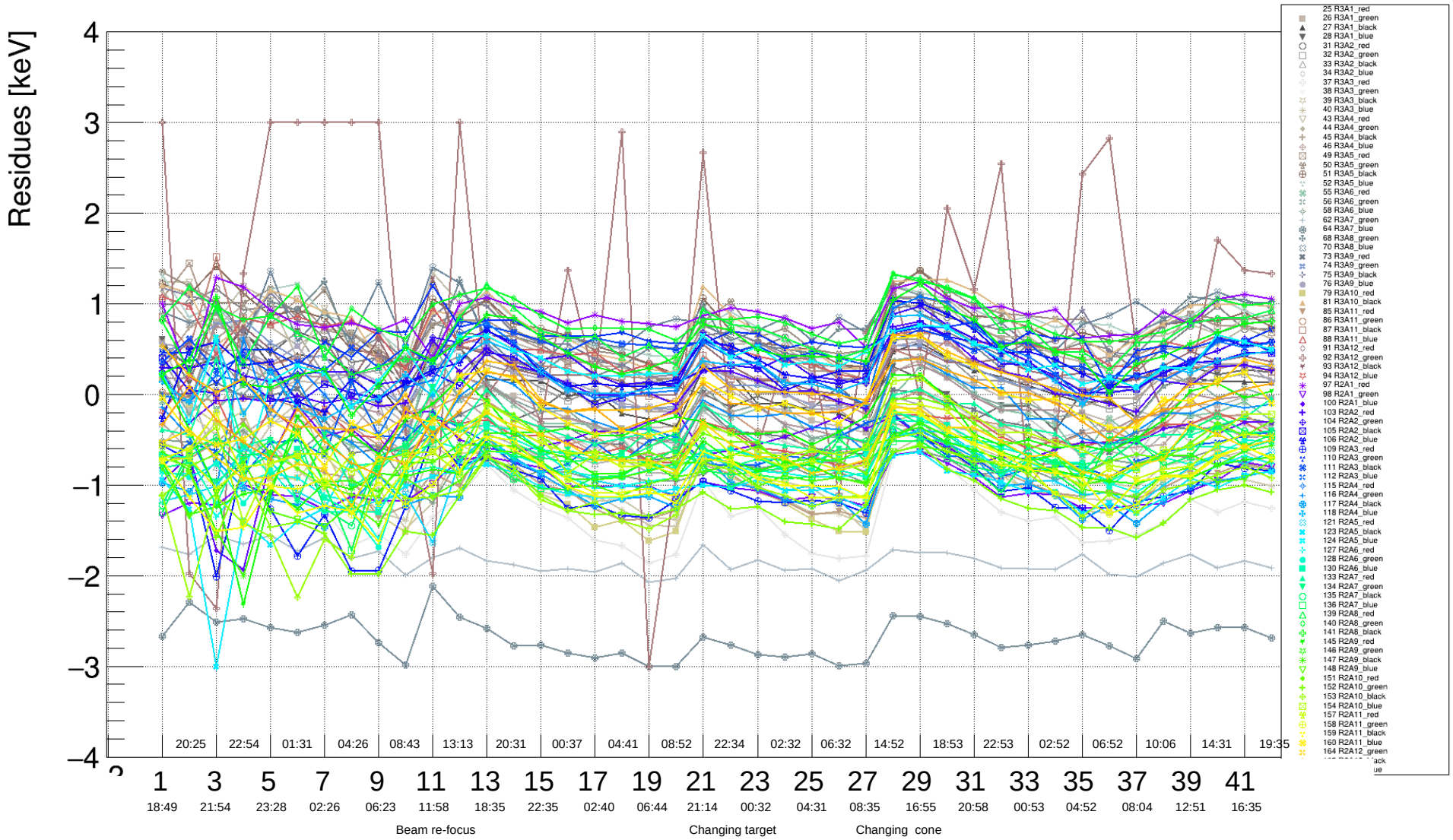
Energy residues with pol1 calibration (152Eu) for energy 810.766000
Residues [keV]
4
3
2
1
0
−1
−2
−3
−4
20:25
22:54
01:31
04:26
08:43
13:13
20:31
00:37
04:41
08:52
22:34
02:32
06:32
14:52
18:53
22:53
02:52
06:52
10:06
14:31
19:35
1 3 5 7 9 11 13 15 17 19 21 23 25 27 29 31 33 35 37 39 41
18:49 21:54 23:28 02:26 06:23 11:58 18:35 22:35 02:40 06:44 21:14 00:32 04:31 08:35 16:55 20:58 00:53 04:52 08:04 12:51 16:35
Beam re-focus
Changing target
Changing cone
25 R3A1_red
26 R3A1_green
27 R3A1_black
28 R3A1_blue
31 R3A2_red
32 R3A2_green
33 R3A2_black
34 R3A2_blue
37 R3A3_red
38 R3A3_green
39 R3A3_black
40 R3A3_blue
43 R3A4_red
44 R3A4_green
45 R3A4_black
46 R3A4_blue
49 R3A5_red
50 R3A5_green
51 R3A5_black
52 R3A5_blue
55 R3A6_red
56 R3A6_green
58 R3A6_blue
62 R3A7_green
64 R3A7_blue
68 R3A8_green
70 R3A8_blue
73 R3A9_red
74 R3A9_green
75 R3A9_black
76 R3A9_blue
79 R3A10_red
81 R3A10_black
85 R3A11_red
86 R3A11_green
87 R3A11_black
88 R3A11_blue
91 R3A12_red
92 R3A12_green
93 R3A12_black
94 R3A12_blue
97 R2A1_red
98 R2A1_green
100 R2A1_blue
103 R2A2_red
104 R2A2_green
105 R2A2_black
106 R2A2_blue
109 R2A3_red
110 R2A3_green
111 R2A3_black
112 R2A3_blue
115 R2A4_red
116 R2A4_green
117 R2A4_black
118 R2A4_blue
121 R2A5_red
123 R2A5_black
124 R2A5_blue
127 R2A6_red
128 R2A6_green
130 R2A6_blue
133 R2A7_red
134 R2A7_green
135 R2A7_black
136 R2A7_blue
139 R2A8_red
140 R2A8_green
141 R2A8_black
145 R2A9_red
146 R2A9_green
147 R2A9_black
148 R2A9_blue
151 R2A10_red
152 R2A10_green
153 R2A10_black
154 R2A10_blue
157 R2A11_red
158 R2A11_green
159 R2A11_black
160 R2A11_blue
164 R2A12_green

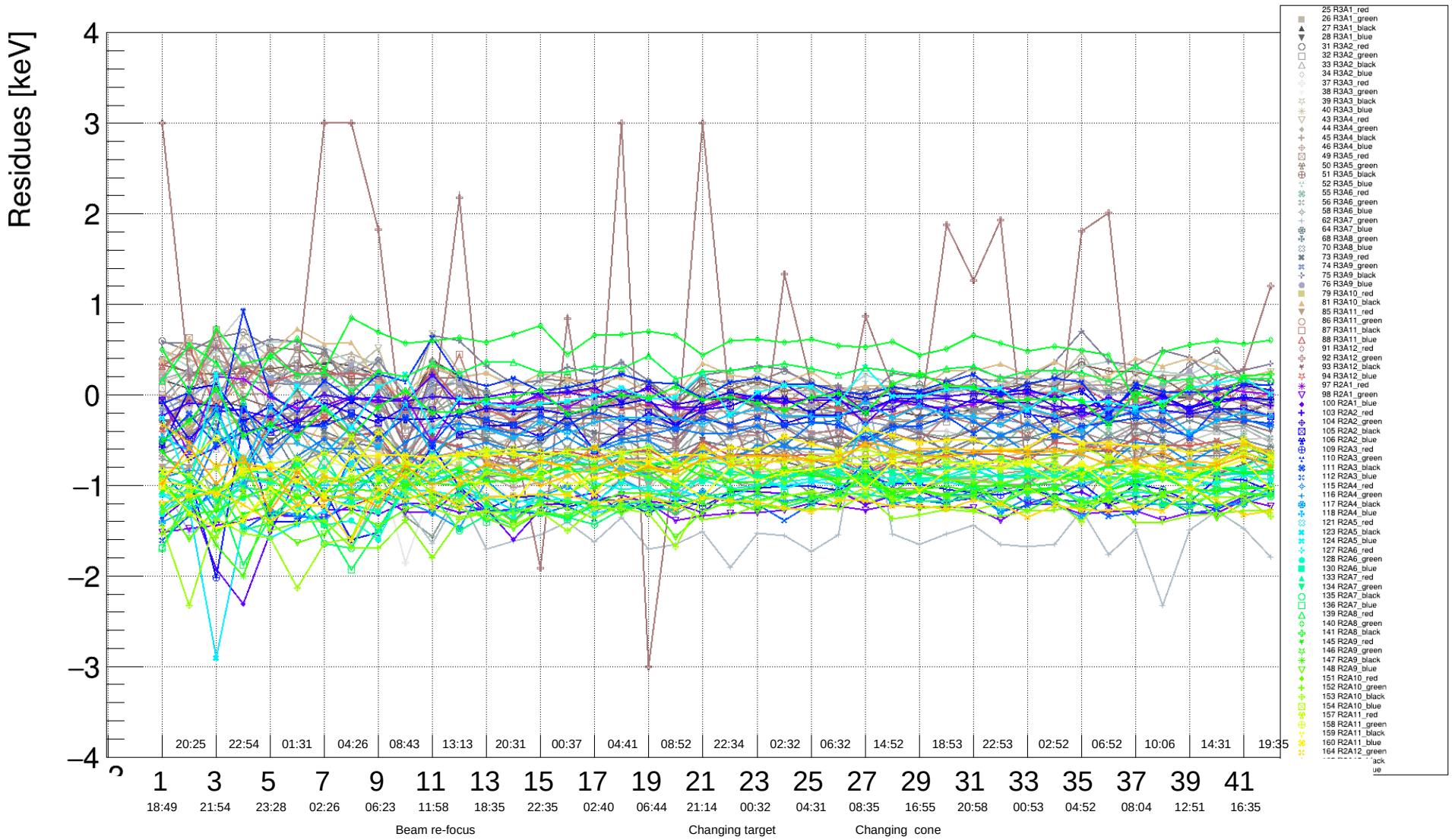
Energy residues with pol1 calibration (152Eu) + run_pol1 for energy 810.766000
Residues [keV]
4
3
2
1
0
−1
−2
−3
−4
20:25
22:54
01:31
04:26
08:43
13:13
20:31
00:37
04:41
08:52
22:34
02:32
06:32
14:52
18:53
22:53
02:52
06:52
10:06
14:31
19:35
1 3 5 7 9 11 13 15 17 19 21 23 25 27 29 31 33 35 37 39 41
18:49 21:54 23:28 02:26 06:23 11:58 18:35 22:35 02:40 06:44 21:14 00:32 04:31 08:35 16:55 20:58 00:53 04:52 08:04 12:51 16:35
Beam re-focus
Changing target
Changing cone
25 R3A1_red
26 R3A1_green
27 R3A1_black
28 R3A1_blue
31 R3A2_red
32 R3A2_green
33 R3A2_black
34 R3A2_blue
37 R3A3_red
38 R3A3_green
39 R3A3_black
40 R3A3_blue
43 R3A4_red
44 R3A4_green
45 R3A4_black
46 R3A4_blue
49 R3A5_red
50 R3A5_green
51 R3A5_black
52 R3A5_blue
55 R3A6_red
56 R3A6_green
58 R3A6_blue
62 R3A7_green
64 R3A7_blue
68 R3A8_green
70 R3A8_blue
73 R3A9_red
74 R3A9_green
75 R3A9_black
76 R3A9_blue
79 R3A10_red
81 R3A10_black
85 R3A11_red
86 R3A11_green
87 R3A11_black
88 R3A11_blue
91 R3A12_red
92 R3A12_green
93 R3A12_black
94 R3A12_blue
97 R2A1_red
98 R2A1_green
100 R2A1_blue
103 R2A2_red
104 R2A2_green
105 R2A2_black
106 R2A2_blue
109 R2A3_red
110 R2A3_green
111 R2A3_black
112 R2A3_blue
115 R2A4_red
116 R2A4_green
117 R2A4_black
118 R2A4_blue
121 R2A5_red
123 R2A5_black
124 R2A5_blue
127 R2A6_red
128 R2A6_green
130 R2A6_blue
133 R2A7_red
134 R2A7_green
135 R2A7_black
136 R2A7_blue
139 R2A8_red
140 R2A8_green
141 R2A8_black
145 R2A9_red
146 R2A9_green
147 R2A9_black
148 R2A9_blue
151 R2A10_red
152 R2A10_green
153 R2A10_black
154 R2A10_blue
157 R2A11_red
158 R2A11_green
159 R2A11_black
160 R2A11_blue
164 R2A12_green

Data presorting – Time alignment

Time alignment is performed individually for each run using a reference detector (LaBr).
The time window in the event building is chosen in order to enhance the signal to background ratio

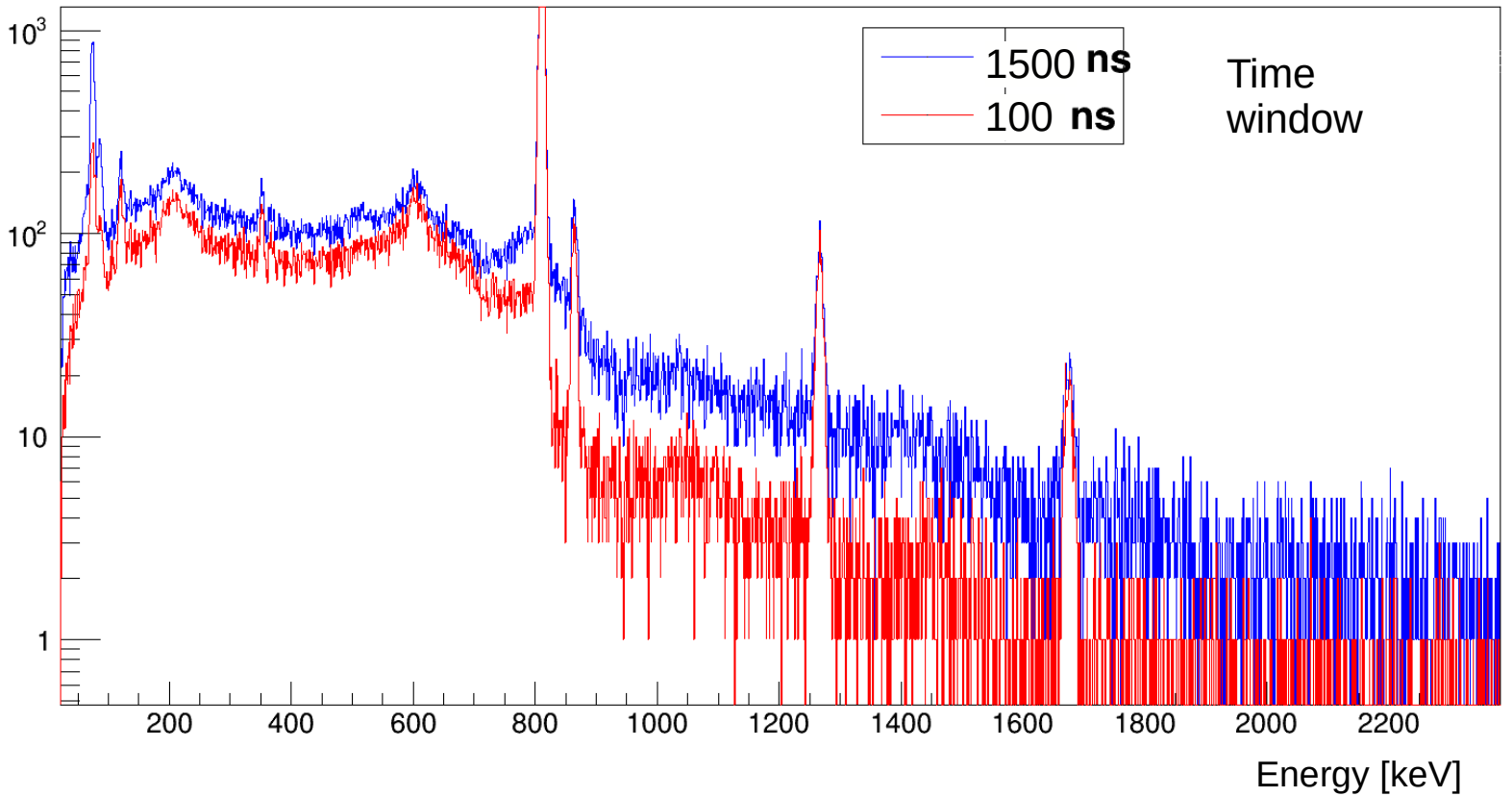

Data presorting – Doppler correction

The gamma rays detected by nuBall are emitted in-flight, when the scattered 58Fe is in motion with a velocity beta from the target to the DSSD. A Doppler correction is needed to create proper energy spectra

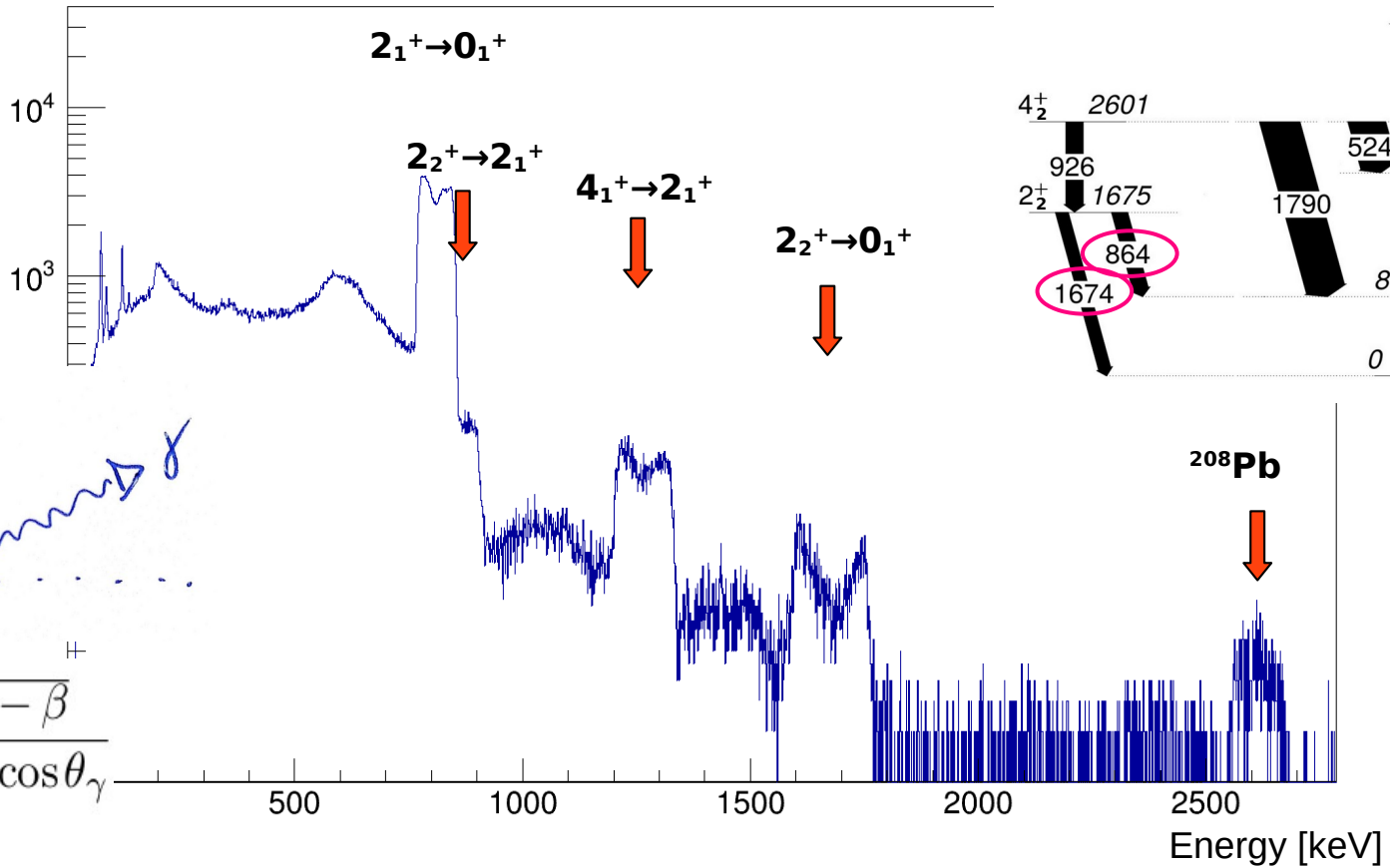

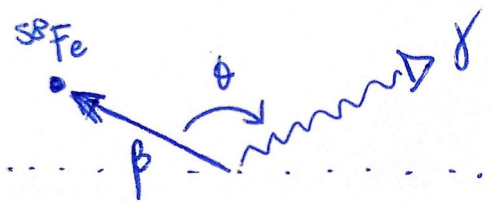

$$E_s = E_\gamma \frac{\sqrt{1-\beta}}{1-\beta\cos\theta_\gamma}$$

Data presorting – Doppler correction

The gamma rays detected by nuBall are emitted in-flight, when the scattered 58Fe is in motion with a velocity beta from the target to the DSSD. A Doppler correction is needed to create proper energy spectra

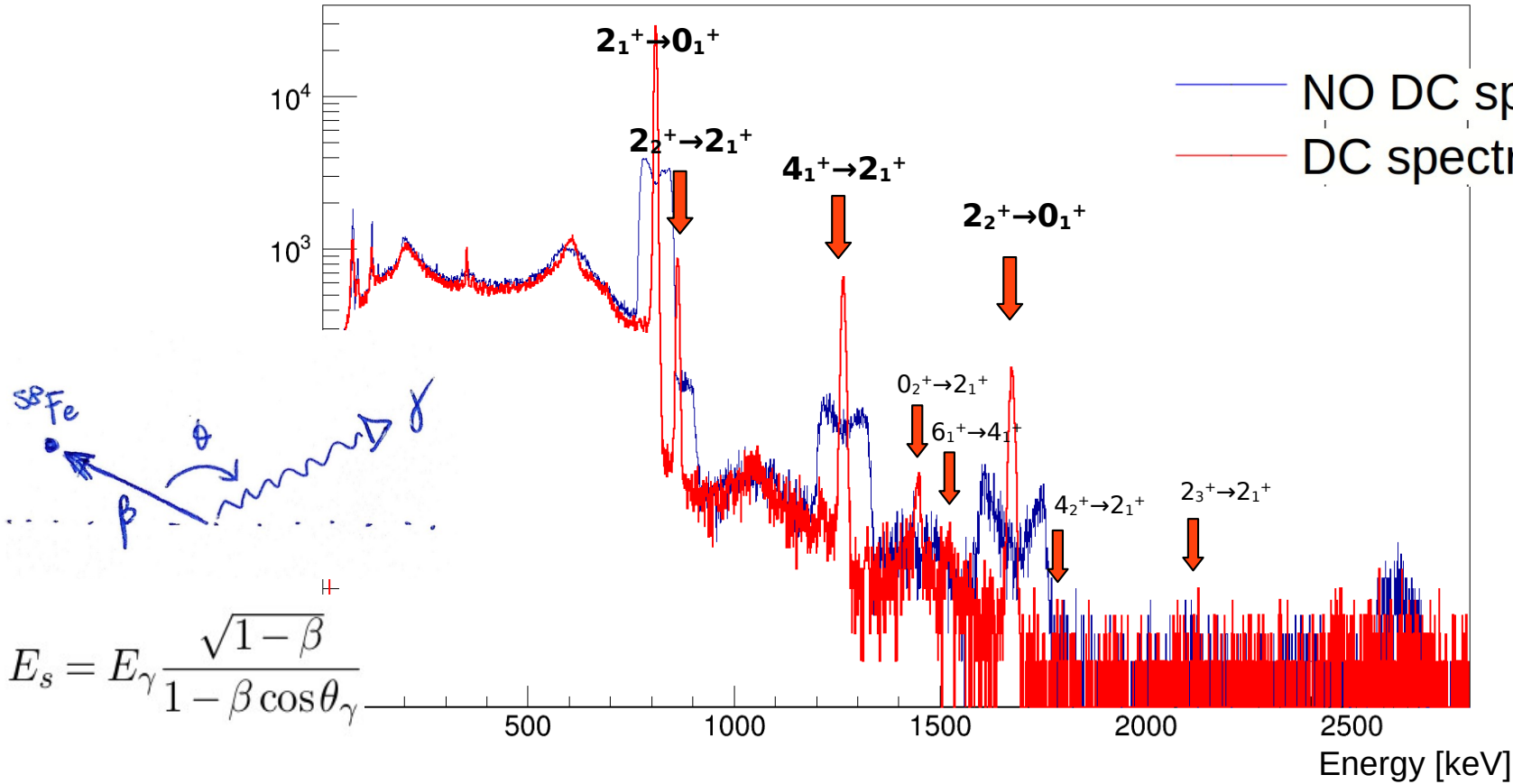

Data presorting – Doppler correction

For the Doppler correction….

- DSSD segment position (32x16)
- Crystal position (96)
- Clover rotation (4)
- Recoil velocity

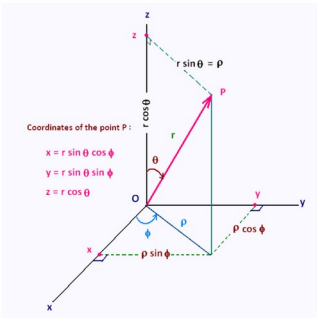

FRAME OF REFERENCE:

To define the geometry, I utilize a spherical coordinate frame of reference, with θ and φ representing angles as depicted in the figure on the right.

During the experiment, the reference frame is rotated to align the z-axis with the direction of the beam. Consequently, the horizontal axis, x, points to the right when facing the incoming beam, while the vertical axis, y, points upward (as illustrated in the figure below).

DSSD:

DSSD lay on a plane x'y' parallel to the xy plane at z_{dTD} = −3.26 cm (distance measured from Doppler corrected data for my experiment).

Each "pad" is defined as the intersection of one ring and one sector and can be univocally determined by a combination of θ and φ (or a set of Cartesian coordinates x,y,z).

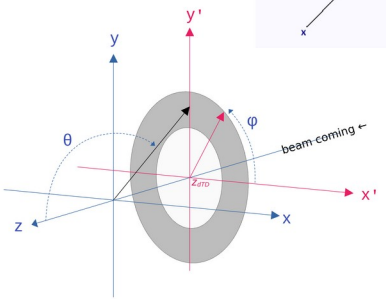

Sectors are labelled from 0 to 31 and ring are labelled from 0 to 15 following the placement in the figure below:

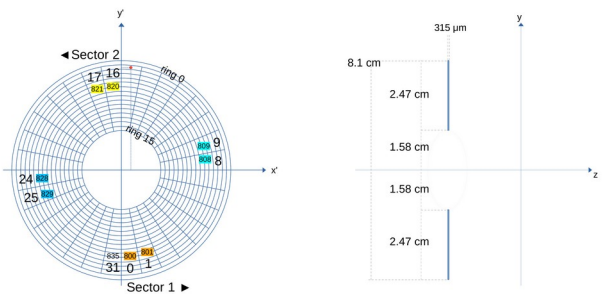

The placement of the DSSD is sensitive to the operator procedure. Therefore, it must be optimized using the data. I adopted a minimization procedure for the sigma of the g.s. transition Doppler-corrected peak, in order to find the correct position of the centre of the DSSD, applying a translation of (dx, dy), and a rotation around the z axis (dφ), as well as for z_{dTD}. As a reference, I found out: dx = −0.14 cm; dy = −0.03 cm; dφ = −0.45 radians.

HPGe:

The Ge crystals are arranged in two rings around the z axis:
- Ring 3 is the one closest to the beam dump
- Ring 2 therefore is the one closest to the beam source.

From my analysis (minimization procedure as for the DSSD positioning, see DSSD section) the centre of the rings, supposed to coincide with the centre of a clover, have theta angles equal to:
- θ_3 = 1.342 radiants (76.9°)
- θ_2 = 1.752 radiants (100.4°)

Clovers are labelled from 0 to 11 for ring 3 and from 12 to 23 for ring 2. The phi (φ) coordinates listed below (in radiants) refer to the centre position of each clover.

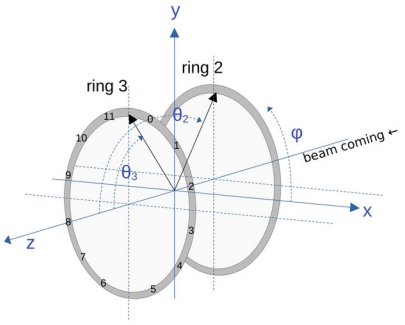

form clover 0 to 11:
1.3089969, 0.78539816, 0.26179939, 6.0213859, 5.497787, 4.974188, 4.45058959, 3.9269908, 3.403392, 2.879793, 2.35619449, 1.8325957
and from clover 12 to 23:
1.3089969, 0.78539816, 0.26179939, 6.0213859, 5.497787, 4.974188, 4.45058959, 3.9269908, 3.403392, 2.879793, 2.35619449, 1.8325957

Each clover is composed of 4 HPGe crystals; the centre position of each crystal has been found with the minimization procedure, optimizing the angle differences from the centre of the corresponding clover (delta_θ, delta_φ). Those are listed in the excel table as well as the θ, φ angles of each clover centre.

Every clover has the same crystals placement (default) except for: clover 5, clover 14, clover 15, clover 17.

Default placement:

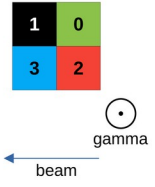

clover 5 (-π/2):

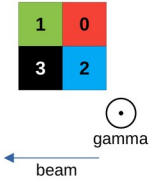

clover 14, 15 (+π/2):

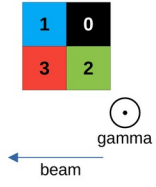

clover 17 (+π):

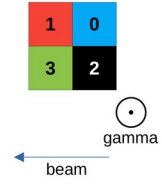

Data presorting – Final spectrum : preliminary *vs* final

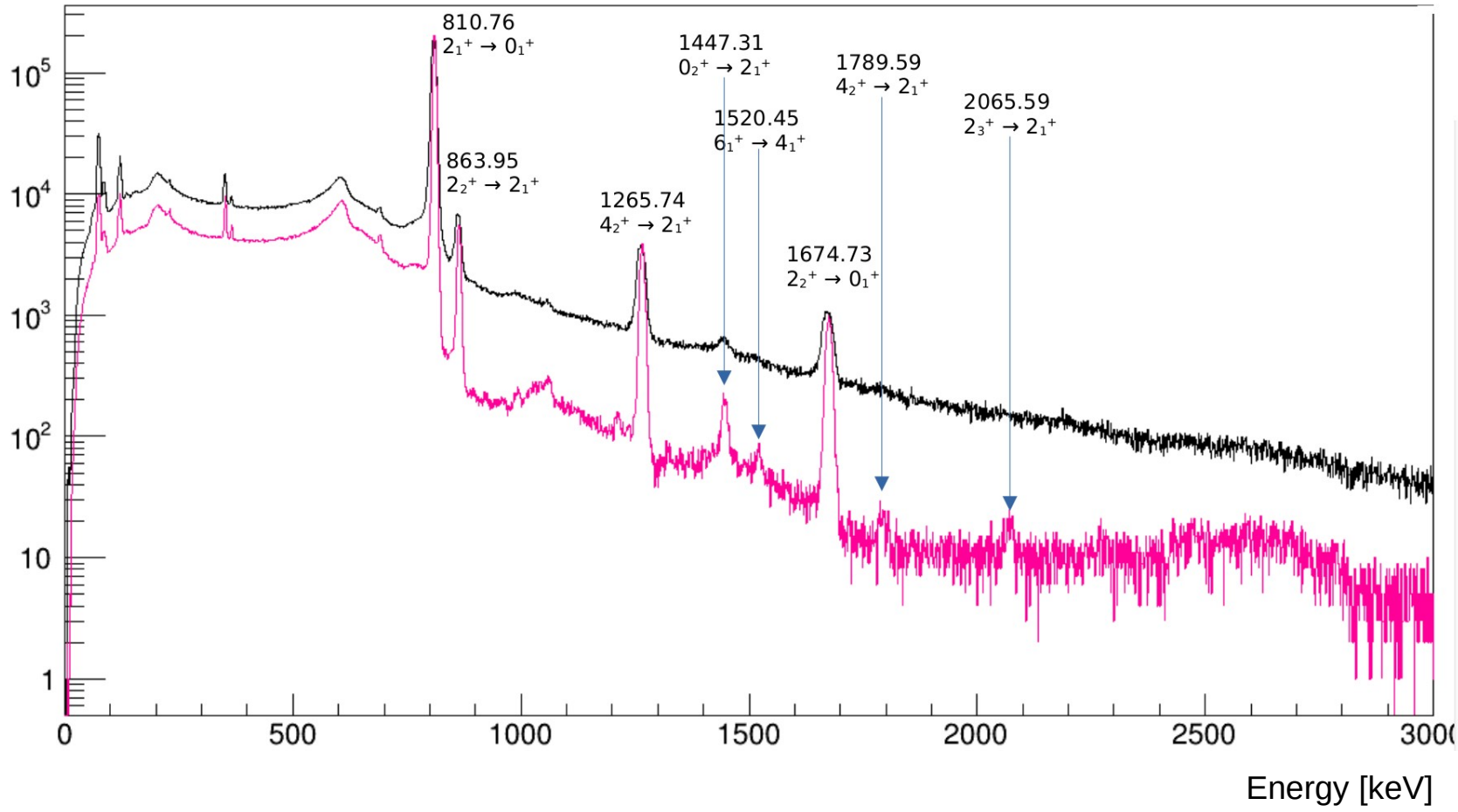

Preliminary results using the GOSIA code

Level scheme used for the GOSIA analysis

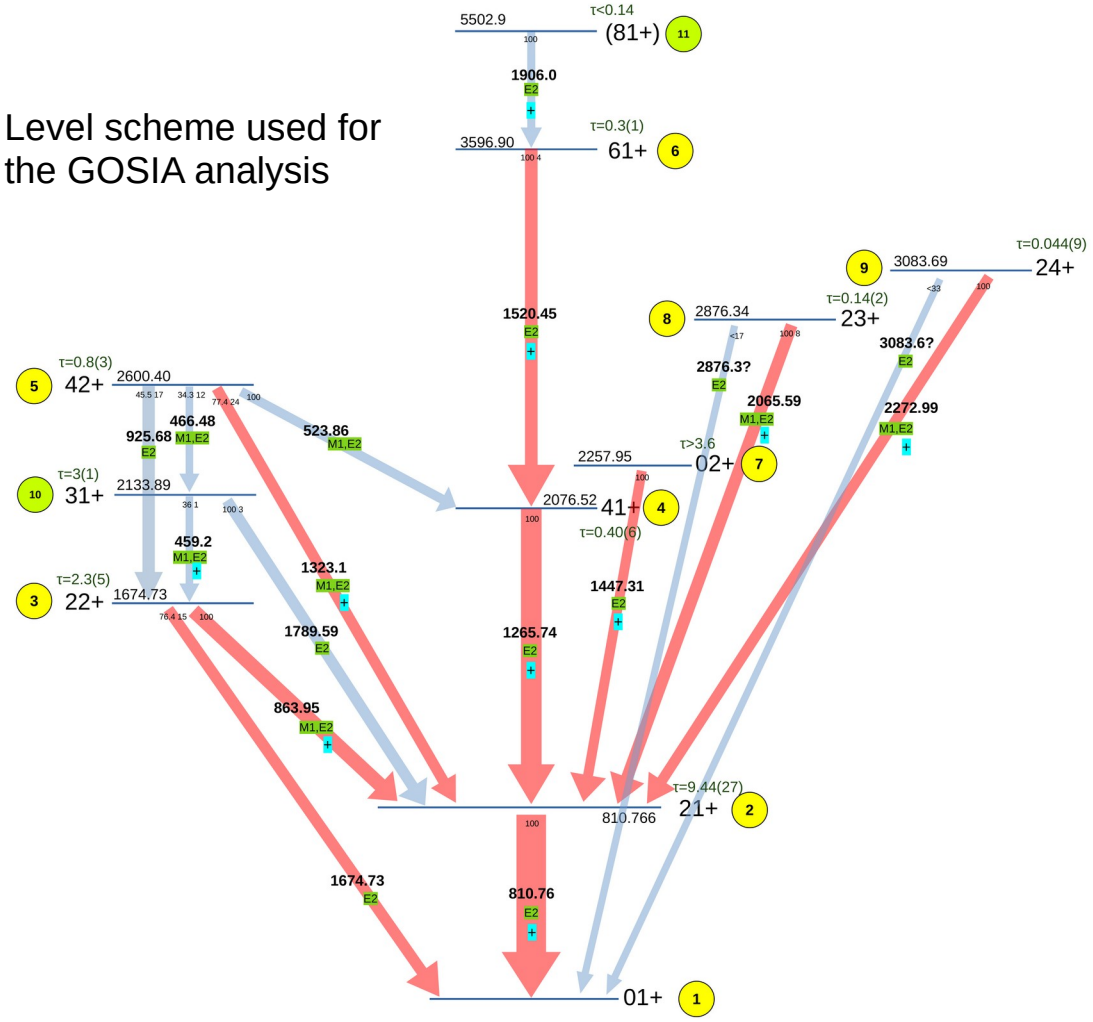

Preliminary results from the all-statistics analysis

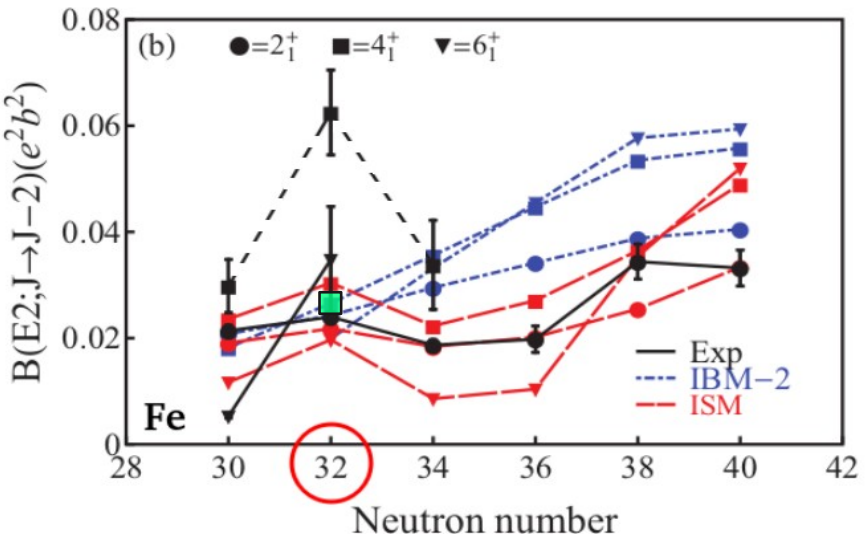

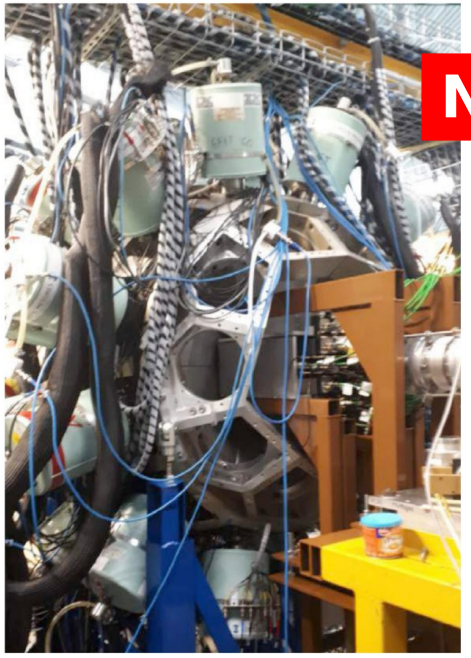

Thanks for your attention!

J. Ljungvall, A. Stuchbery, S. Bottoni, G. Charles, E. Cantacuzene, K. Desislava, K. Hauschild, C. Hiver, K. Hadyńska-Klęk, M. Iolanda, M. Kaci, M. Komorowska, M. Lebois, S. Lenzi, N. Marchini, M. Matejska-Minda, A. Lopez-Martens, P. Garrett, A. Goasduff, P.J. Napiorkowski, S. Panasenko, M. Rocchini, T.R. Rodríguez, M. Siciliano, K. Stoychev, J. Wilson, K. Wrzosek-Lipska, M. Zielinska